Effects of Particle Size on the Molecular Orientation and Birefringence of Magnetic Nanoparticles/Polyimide Composites

Jin Ho Kang, Young Chul Kim, Kilwon Cho, Chan Eon Park

Department of Chemical Engineering, Division of Electrical Computer Engineering, Research Center for Catalytic Technology, Research Polymer Research Institute, Pohang University of Science and Technology, Pohang, South Korea 790−784

ABSTRACT: Size dependency of nanoparticles for birefringence and molecular orientation of nanocomposite films have been studied using a prism coupler and near-edge X-ray absorption fine structure spectroscopy (NEXAFS). We synthesized two different sizes of magnetic nanoparticles, $Ni_{0.6}Zn_{0.4}Fe_2O_4$. The smaller ones were 6.1 ± 1.3 nm-diameter nanoparticles showing superparamagnetism and the larger ones were 20.7 ± 6.1 nm-diameter nanoparticles showing ferrimagnetism. To make nanocomposites, we incorporated these particles into poly(N,N'-bis(phenoxyphenyl)pyromellitimide) (PMDA-ODA PI). From the prism coupler study, pristine PI without nanoparticles had higher out-of-plane birefringence, which indicated high in-plane orientation of polyimide. However, the birefringence of PI nanocomposites decreased with the increase of particle content. The birefringence of PI nanocomposite with small nanoparticles was smaller than that of PI nanocomposite with large nanoparticles. The birefringence of PI nanocomposite with 1 wt % of small nanoparticles was reduced to almost half of that of pristine PI due to the decreased orientation of PI molecules. NEXAFS spectra of N K-edge were the same as the birefringence results. Imide and phenyl rings of pristine PI aligned more parallel to the in-plane direction, but those of PI with nanoparticles aligned less parallel to the in-plane direction. © 2006 Wiley Periodicals, Inc. J Appl Polym Sci 99: 3433–3440, 2006

Key words: polyimides; nanocomposites; molecular orientation; birefringence; NEXAFS

INTRODUCTION

Nanostructure materials have been extensively studied worldwide in the past few years.[1] Owing to their small size, nanoscale materials exhibit unique physical and chemical properties that are different from their bulk state.[2] Many reports on quantum size effects on semiconductor[3–5] and emergence of unique properties with the particles size[6–8] have been published during the past decade.

In these various nanostructure materials, magnetic nanoparticles and magnetic nanocomposites have a wide range of applications, for example, information storage,[9] color imaging,[10] magnetic refrigeration,[11] ferrofluids,[12] cell sorting,[13] medical diagnosis,[14] controlled drug delivery,[15] magneto-optical devices,[16] and so forth.

Among the most attractive properties of magnetic nanocomposites, magneto-optical effects are very important in such areas as integrated optical devices, optical fiber, and sensors.[17] Several authors have reported on the synthesis and Kerr effect of γ-Fe_2O_3 and Fe/SiO_2 magnetic nanocomposite by sol–gel methods.[18–20] Some magnetic properties such as saturation magnetization, remanent, and coercivity of magnetic/polymer nanocomposite have been measured.[21]

Polyimide (PI) nanocomposites are expected to offer many advantages such as high thermal stability, superior chemical resistance, and low dielectric constant.[22] However, PI has large birefringence, which restrict its use for a polarized beam for integrated optical devices.[23] Thus, molecular chain orientation of PI is very important. There have been some studies on the content-effect of imbedded microsized (about 1-μm) particles on the birefringence.[24–26] Chang et al. synthesized poly(BPDA-ODA)/silica hybrid optical thin films using the sol–gel method, and reported that the birefringence of hybrid PI films with 15.6 wt % of silica particles was reduced to half of that of pristine PI.[24] However, it needed too much incorporated nanoparticles to reduce the birefringence, and there has been no research about the size-effect of imbedded

nanoparticles on the birefringence and the molecular chain orientation.

In this study, we synthesized two different PI nanocomposites having different sized nanoparticles. Also, the effects of size and content of imbedded nanoparticles on birefringence and molecular chain orientation of PI were investigated using a prism coupler and near-edge X-ray absorption fine structure spectroscopy (NEXAFS).

EXPERIMENTAL

Preparation of magnetic nanoparticles

Two different sizes of magnetic nanoparticles, $Ni_{0.6}Zn_{0.4}Fe_2O_4$, were synthesized: One was about 6 nm-diameter and the other was about 20 nm-diameter. Small magnetic nanoparticles (~6 nm) were synthesized from functionalized surfactants.[27–30] The functionalized anionic surfactants, with metal counter ions, were synthesized by the following method: Aqueous solution of $0.1M$ sodium dodecylsulfate (SDS) was mixed with aqueous solution of $0.1M$ of iron chloride, nickel chloride, and zinc chloride at 25°C. The mixed solution was chilled to 2°C to precipitate. This precipitate was washed several times with iron chloride, nickel chloride, and zinc chloride aqueous solution and recrystallized in distilled water. The products are iron dodecylsulfate, $Fe(DS)_2$, nickel dodecylsulfate, $Ni(DS)_2$, and zinc dodecylsulfate, $Zn(DS)_2$.[31]

$Fe(DS)_2$, $Ni(DS)_2$, $Zn(DS)_2$, and dodecyltrimethylammonium chloride (DTAC) were dissolved in deionized water at the mole ratio of 2:0.6:0.4:0.75 to synthesize $Ni_{0.6}Zn_{0.4}Fe_2O_4$ nanoparticles. DTAC was used as a cationic surfactant giving an ellipsoidal micellar morphology.[32] Methylamine ($0.7M$) was added to this solution and mixed for 6 h at 25°C under air atmosphere to form magnetic nanoparticles. The magnetic nanoparticles were removed by centrifugation and washed several times. To obtain dry powder, the solvent was removed by freeze-drying. The particles were dissolved ultrasonically in N-methylpyrrollidone (NMP) with a small amount of HNO_3 aqueous solution to prepare a magnetic fluid. A small amount of HNO_3 endowed the surface charges on the particles for homogeneous dispersion.

On the other hand, large magnetic nanoparticles (~20 nm) were synthesized by a similar Massart method without any surfactant.[33] The large particles were obtained by mixing metal chloride aqueous solution with $0.7M$ aqueous solution of methylamine without any surfactants. These reaction products were washed five times with acetone and $1.0M$ nitric acid, and then centrifuged at 3000 rpm for 30 min. These particles also were dissolved ultrasonically in NMP to prepare a magnetic fluid with a small amount of HNO_3 aqueous solution.
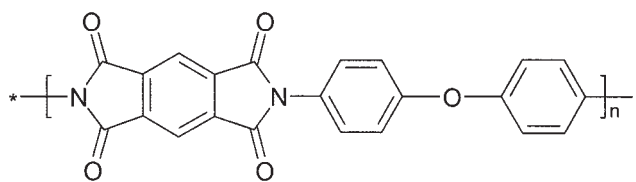

Figure 1 Schematic diagram of the poly(N,N'-bis(phenoxyphenyl)pyromellitimide) (PMDA-ODA PI).

Preparation of poly(amic acid)

Poly(N,N'-bis(phenoxyphenyl)pyromellitimide)(PMDA-ODA PI) was synthesized from 4,4'-oxydianiline (ODA) as diamine and pyromellitic dianhydride (PMDA) as dianhydride (Fig. 1). ODA (Wakayama Seika Kogyo Co., Japan) and PMDA (Daicel Co., Japan) were taken out of bottles in a glove box under an argon atmosphere and used immediately without any refining. Anhydrous N-methylpyrrollidone (NMP, Aldrich Chemical, US) was used as solvent without further purification. The reaction was conducted for 8 h with stirring at about 10°C in N_2 atmosphere. To control the molecular weight of poly(amic acid), it was kept in a convection oven at 80°C to obtain about 25,000 centipoise of viscosity.

Preparation of magnetic nanoparticles/polyimide composites

To prepare magnetic nanoparticles/polymer composites, poly(amic acid) solution was mixed with an adequate amount of magnetic fluid. Magnetic particle contents were 0.1, 0.3, 0.5, 1, and 5 wt % in nanocomposites. Nanocomposite precursor was spin-coated on silicon wafer (100 P-type) and prebaked at 100°C for 1 h and cured at 150°C for 30 min, 200°C for 30 min, 300°C for 1 h, and 400°C for 1 h. The heating rate was 5°C/min up to 200°C and 2°C/min up to 400°C

Nomenclature of the PI nanocomposite is PI-S/L-X. S/L and X represent nanoparticle size (S: small, L: large) and nanoparticle content (wt %), respectively. For example, PI-S-0.5 represents the PI nanocomposite with 0.5 wt % of 6 nm-diameter nanoparticles, and PI-L-1 represents the PI nanocomposite having 1 wt % of 20 nm-diameter nanoparticles.

Bulk characterization of magnetic nanoparticles and magnetic nanoparticles/polymer composites

The particles floated on a 300 mesh carbon-coated copper grid were observed with a transmission electron microscopy (TEM, Model H-7600, Hitach) operated at 110 kV. Cross-sectional views of nanocomposite films were observed after cutting with microtome (MT-7000, Research and Manufacturing Co.). X-ray diffraction measurements were carried out with the

TABLE I
Critical Micelle Concentration of Anionic Surfactant with Different Metal Counter Ions

	Critical micelle concentration (mol/L)	
Surfactant	25°C	50°C
SDS	0.00080	0.00089
$Fe(DS)_2$	0.00141	0.00252
$Ni(DS)_2$	0.00137	0.00250
$Zn(DS)_2$	0.00135	0.00180

8C1 beam line of Pohang Accelerator Laboratory (PAL, $\lambda = 1.54056$ Å). The magnetic properties of the samples were measured using a home-made vibrating sample magnetometer (VSM) at room temperature up to an 8 kOe of magnetic field. For measuring birefringence of nanocomposite films, a home-made prism coupler was used with a He–Ne laser source. Prism coupling patterns were measured in transverse electric (TE: $n_{xy} = n_{TE}$, the refractive index in a film plane) and transverse magnetic (TM: $n_z = n_{TM}$, the refractive index out of a film plane) modes by choosing the appropriate polarization of the incident laser beam as described elsewhere.[34–36] The average refractive index (n_{ave}) and the out-of-plane birefringence (Δn) in films were estimated from the measured refractive indices

$$n_{ave} = \frac{(2n_{xy} + n_z)}{3} \qquad (1)$$
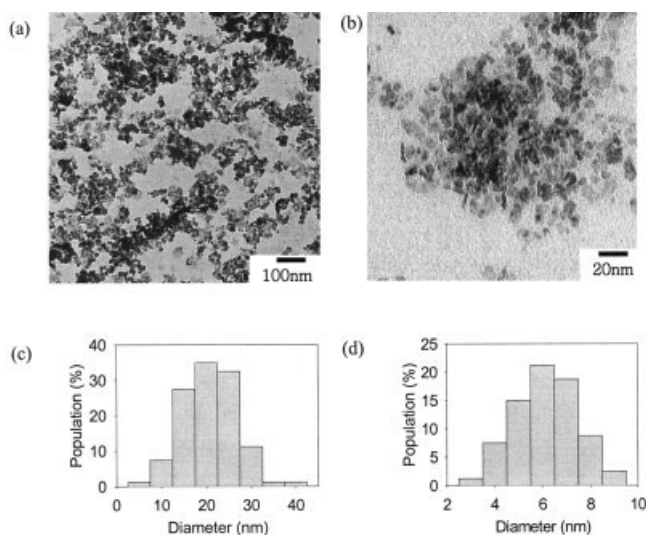
$$\Delta n = n_{xy} - n_z \qquad (2)$$

Figure 2 TEM morphology and histograms of $Ni_{0.6}Zn_{0.4}$-Fe_2O_4 nanoparticles. Top panel: TEM morphology of nanoparticles synthesized (a) without surfactant and (b) with mixed surfactants. Note the length-scale difference in (a) and (b); Bottom panel: Histogram of nanoparticles synthesized (c) without surfactant and (d) with mixed surfactants.
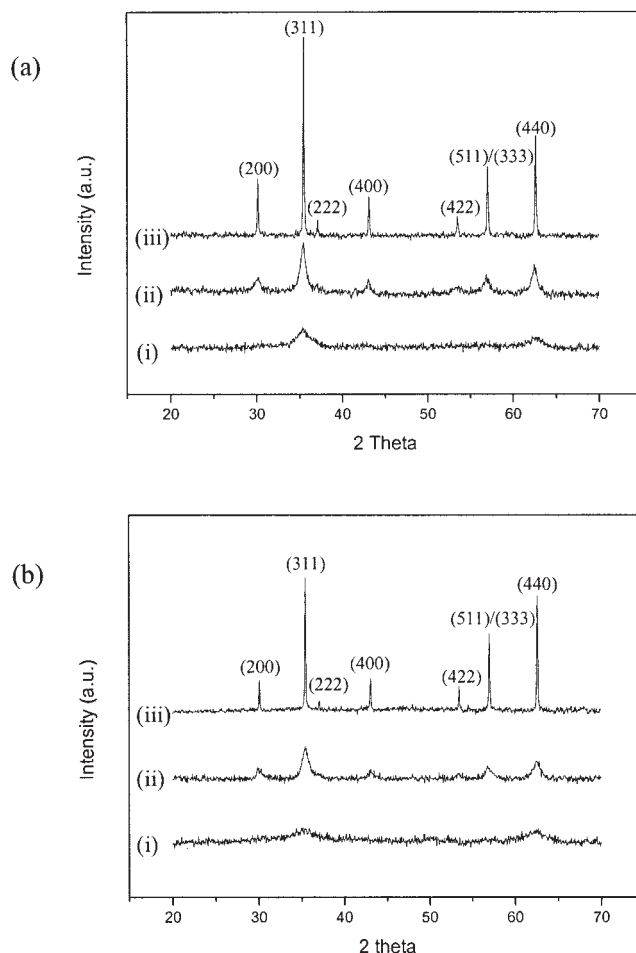
Figure 3 X-ray diffraction pattern of $Ni_{0.6}Zn_{0.4}Fe_2O_4$ nanoparticles synthesized (a) without surfactant and (b) with mixed surfactant: (i) as synthesized; (ii) after annealing at 400°C; and (iii) after annealing at 800°C.

All measurements were performed using a cubic zirconia prism of $n_{TE} = n_{TM} = 2.1677$ at a wavelength of 632.8 nm (i.e., 474.08 THz). All the samples were controlled to have the same thickness of about 1 μm.

Surface characterization of magnetic nanoparticles/polyimide composite films by NEXAFS

For NEXAFS studies, nanocomposite precursor solution was spin-coated on a gold-coated silicon wafer (100 p-type, $Au/Ti/SiO_2/Si$ wafer, Au 100 nm, Ti 10 nm, and SiO_2 300 nm). They were cured at 400°C for 1 h to obtain fully imidized PI nanocomposite. Total electron yield (TEY) X-ray absorption experiments have been carried out with the 2B1 beam line of Pohang Accelerator Laboratory (PAL) with a resolution better than 0.2 eV at the nitrogen K-edge electron.[37,38] All the spectra have been normalized by dividing the electron yield signal from a reference gold-coated grid monitor.[37,38] Reproducibility of the spectra has been checked by multiple scanning. The information depth
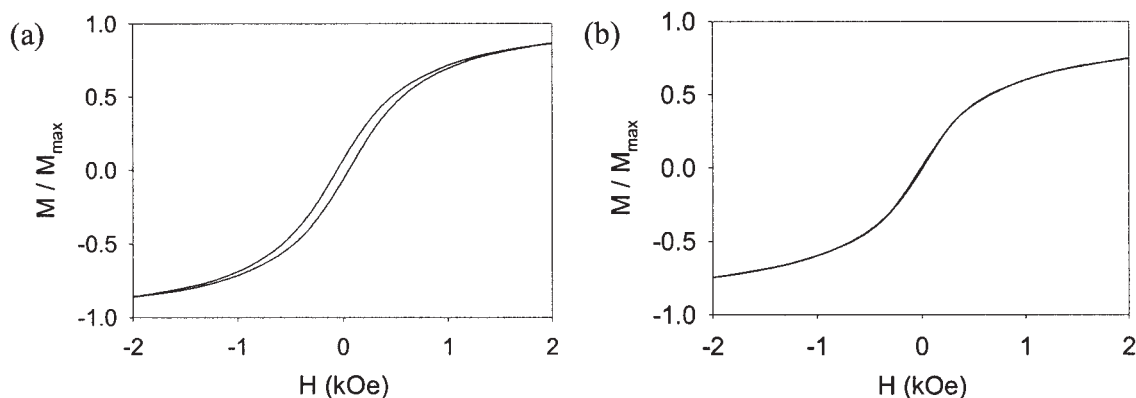
Figure 4 Magnetization of $Ni_{0.6}Zn_{0.4}Fe_2O_4$ nanoparticles as a function of applied magnetic field at room temperature synthesized (a) without surfactant and (b) with mixed surfactants.

of the NEXAFS can be estimated to be <10 nm.[38] To investigate the orientation of PI molecules, the two different angles of incidence of the linearly polarized synchrotron light were used: 90° (electric field vector E lies parallel to the in-plane direction) and 20° (E is 70° to the in-plane direction).

RESULTS AND DISCUSSION

Synthesis of magnetic nanoparticles and nanocomposites

Critical micelle concentration (CMC) of anionic surfactants for 6-nm magnetic nanoparticles was measured by the maximum bubble pressure method at 25 and 50°C. CMCs of SDS were 8.0×10^{-4} mol/L at 25°C and 8.9×10^{-4} mol/L at 50°C, which was consistent with other literature.[32] The CMCs of $Fe(DS)_2$, $Ni(DS)_2$, and $Zn(DS)_2$ were larger than those of SDS (Table I). The counter ions of Fe, Ni, and Zn increased the charge density on the polar group of the surfactants,

inducing the polar repulsion between surfactants and the increase of CMC.[32] CMCs at 50°C were larger than those at 25°C, because the increase in temperature reduced the hydrophobic attraction of hydrophobic groups of surfactants.[32]

From the study of small-angle X-ray spectroscopy (SAXS), the micelles of functionalized anionic surfactants with metal-counter ions were ~50 Å-diameter and uniform prolate ellipsoids.[39] Similarly, the nanoparticles synthesized from mixed surfactants were ellipsoidal particles with the size of 6.1 ± 1.3 nm (Figs. 2(b) and 2(d)). On the other hand, nanoparticles synthesized without any surfactant were large, 20.7 ± 6.1 nm diameter (Figs. 2(a) and 2(c)). The X-ray diffraction pattern of magnetic nanoparticles with various annealing times showed the inverted spinel crystalline structure (Fig. 3).[30] Higher annealing temperature showed higher crystallinity of nanoparticles.

The magnetization curves of these nanoparticles annealed at 400°C were obtained at room temperature
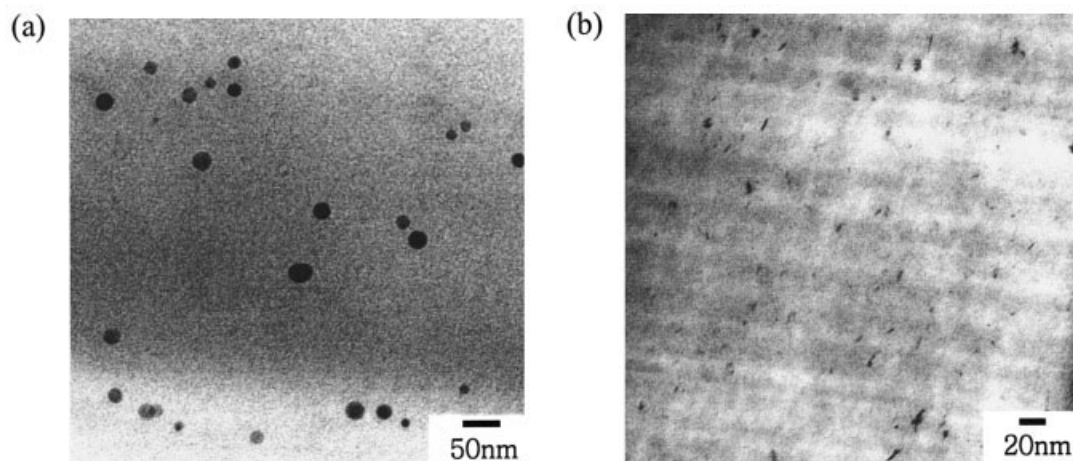

Figure 5 TEM morphology of cross-sectional view of PI nanocomposite film having $Ni_{0.6}Zn_{0.4}Fe_2O_4$ synthesized (a) without surfactants (PI-L-1) and (b) with mixed surfactants (PI-S-1).

TABLE II
Refractive Index of $Ni_{0.6}Zn_{0.4}Fe_2O_4$/PI Nanocomposites Films

Particles contents (wt %)	PI-L series				PI-S series			
	n_{TE}	n_{TM}	n_{ave}	Δn	n_{TE}	n_{TM}	n_{ave}	Δn
0	1.735	1.626	1.699	0.109	1.735	1.626	1.699	0.109
0.1	1.750	1.647	1.716	0.103	1.737	1.661	1.711	0.076
0.3	1.752	1.656	1.720	0.096	1.739	1.665	1.714	0.074
0.5	1.759	1.666	1.728	0.093	1.740	1.664	1.715	0.076
1	1.761	1.675	1.732	0.086	1.742	1.676	1.720	0.066
5	1.780	1.712	1.757	0.068	1.755	1.713	1.741	0.042

(Fig. 4). The saturation magnetization, Ms was not reached even with 8 kOe magnetic field in the both case of samples. The maximum magnetization of 20 and 6 nm nanoparticles were 21.5 and 12.3 emu/g, for 8 kOe, respectively.

Coercivity of 20 nm nanoparticles was 61 Oe but that of small nanoparticles was zero. Six nanometer nanoparticles were superparamagnetic particles. When particles are smaller than single magnetic domain (~10 nm), they show superparamagnetic behavior with no reduced remanence and coercivity.[40] However, large nanoparticles, which were larger than magnetic domain, showed ferrimagnetic behavior. The cross-sectional TEM morphology of PI nanocomposite films showed the homogeneously dispersed nanoparticles (Fig. 5).

Refractive indices of magnetic nanoparticles/polyimide composite films

Pristine PI without nanoparticles had the in-plane refractive index (n_{TE}) of 1.735, the out-of-plane refractive index (n_{TM}) of 1.626, the average refractive index (n_{ave})
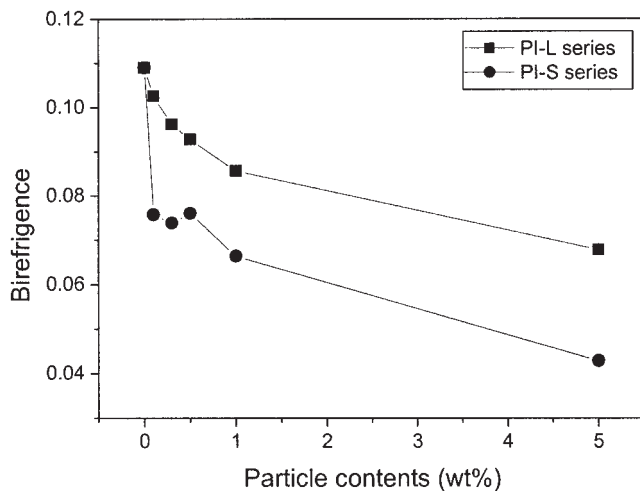
Figure 6 Birefringence of $Ni_{0.6}Zn_{0.4}Fe_2O_4$/PI nanocomposites films.
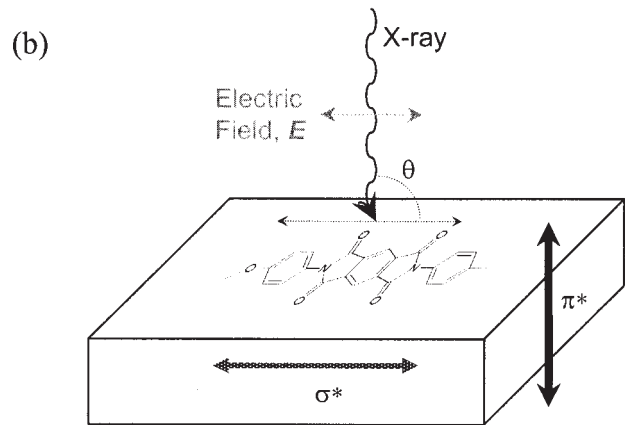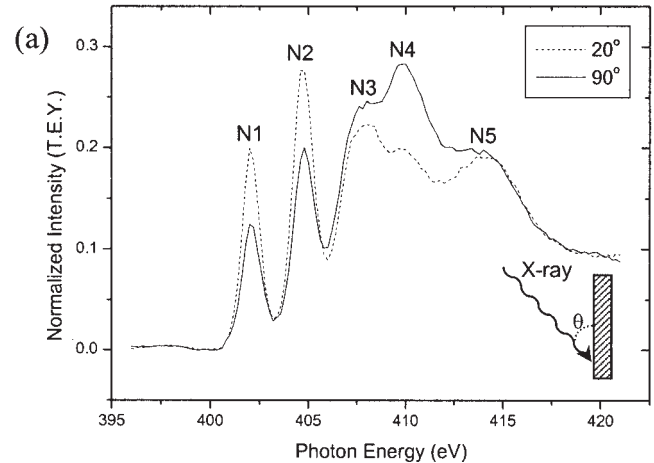
Figure 7 Nitrogen K-edge total electron yield spectrum of homo PI (a) and a schematic diagram of PI film showing σ^* and π^* bond orbital directions (b).

of 1.699, and the out-of-plane birefringence (Δn) of 0.109. PI films, which were spin-coated on silicon wafer and imidized, had generally higher refractive index in the film plane than out-of-plane, and the in-plane refractive index (n_{TE}) was isotropic within the film plane ($n_x = n_y = n_{xy} = n_{TE}$).[34] Therefore, the out-of-plane birefringence ($\Delta n = n_{TE} - n_{TM}$) of films was used to estimate the degree of molecular in-plane orientation.[34–36]

TABLE III
Assignments of Resonance Peaks in the N K-edge NEXAFS Spectra for Nanocomposite Films

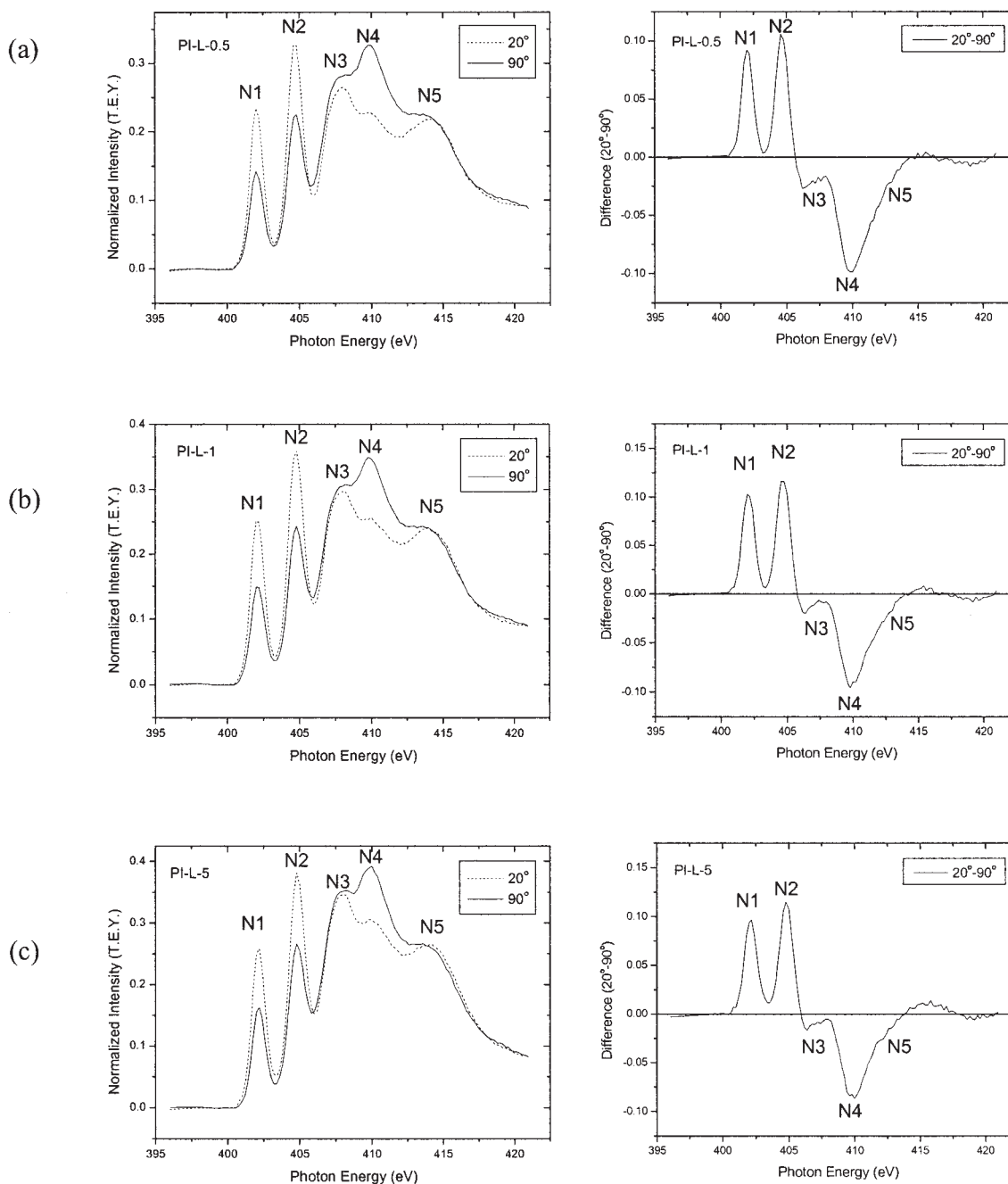| Peak	Photon energy (eV)	Final orbital state
N1	402.0	π^* (imide ring)
N2	404.6	π^* (imide ring)
N3	407.8	π^* (C—N), σ^* (C—N)
N4	409.8	σ^* (C—N)
N5	413.8	σ^* (C—C)

Figure 8 Nitrogen K-edge total electron yield spectrum of (a) PI-L-0.5, (b) PI-L-1, and (c) PI-L-5.

The refractive index of $Ni_{0.6}Zn_{0.4}Fe_2O_4$ nanoparticles was estimated to be very high because of its high relative permittivity and permeability ($\varepsilon_r > 100$, $\mu_r > 2000$ at 1 MHz, and $n^2 = \varepsilon\mu$).[41,42] Thus, the refractive indices (n_{TE}, n_{TM}, and n_{ave}) of PI-L and PI-S series increased with the increase of particle content.

Although n_{TM} of the PI-L series were almost the same as that of the PI-S series, n_{TE} and n_{ave} of the PI-L series were larger than those of the PI-S series, as shown in Table II. This indicates that the smaller nanoparticles hindered the in-plane orientation of PI more

than the larger nanoparticles due to the larger number of particles: at the same particle content, there were about 37 ($\approx (20/6 \text{ nm})^3$) times more particles in the nanocomposite with the smaller particles.

As shown in Figure 6, the out-of-plane birefringences of the PI-L series decreased monotonously as a function of the particle content, and were larger than those of PI-S series. The out-of-plane birefringences of the PI-S-0.1, having just 0.1 wt % of nanoparticles, were much smaller than those of pristine PI. Furthermore, the birefringence of PI-S-1 reduced to almost half of that of pristine PI.
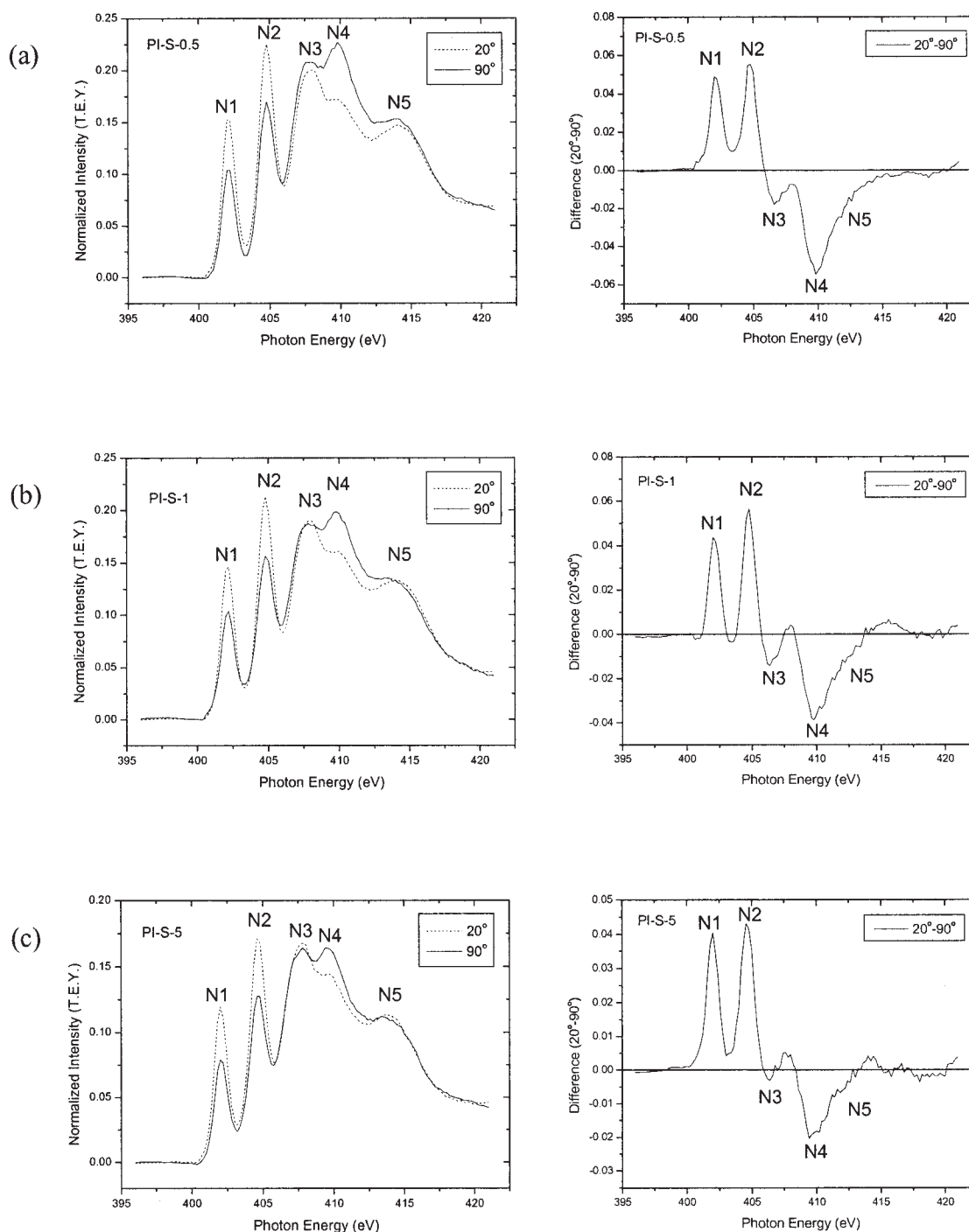
Figure 9 Nitrogen K-edge total electron yield spectrum of (a) PI-S-0.5, (b) PI-S-1, and (c) PI-S-5.

Molecular orientation of magnetic/polyimide nanocomposite films

Figure 7 shows nitrogen K-edge NEXAFS spectra of pristine PI. The first sharp peaks, labeled N1 and N2 at 402.0 and 404.6 eV, respectively, correspond to the excitation of $N_{1\,s}$ core electrons into empty π^* bond orbitals of imide ring and phenyl ring, respectively, as assigned in Table III.[43] The intensities of these resonance peaks for 90° of incident angle of X-ray beam were smaller than those for 20° of incident angle, which meant that the π^* bond orbital was approximately perpendicular to the in-plane direction. The N4, σ^* bond orbital resonance peaks for 90° of incident angle were larger than those for 20° of incident angle, which meant that the σ^* bond orbital was parallel to the in-plane direction. These σ^* and π^* bond orbital resonance spectra indicate that imide and phenyl rings of PI aligned approximately parallel to the in-plane direction (Fig. 7(b)).

The nitrogen K-edge NEXAFS spectra of PI-L-0.5 was almost the same as that of pristine PI (Fig. 8(a)). The differences of the peaks between 90° of incident angle and 20° of incident angle for N1, N2, N3, N4, and N5 decreased with the increase of particle content in the case of PI-L series (Fig. 8). These changes of peaks were more pronounced in the case of PI-S series compared to pristine PI (Figs. 7 and 9). This indicates that imide and phenyl ring planes of PI nanocomposites with smaller particles were more randomly oriented. The peaks for σ^* bond orbitals, N3, N4, and N5 showed much more pronounced changes rather than those for π^* bond orbitals.

CONCLUSIONS

To examine the effect of size and content of imbedded nanoparticles on the birefringence and the molecular orientation of PI nanocomposite films, we synthesized two different sizes of $Ni_{0.6}Zn_{0.4}Fe_2O_4$ nanoparticles. One was 6.1 ± 1.3 nm-diameter and the other was 20.7 ± 6.1 nm-diameter. Small nanoparticles were synthesized from functionalized anionic surfactants, with metal counter ions, and large magnetic nanoparticles were synthesized without any surfactant. Coercivity of large nanoparticles was 61 Oe, showing ferrimagnetism, but that of small nanoparticles was zero, showing superparamagnetism. To make PI nanocomposites, these particles were incorporated into poly(N,N'-bis(phenoxyphenyl)pyromellimide) (PMDA-ODA PI).

From the prism-coupler study, pristine PI had high out-of-plane birefringence (Δn) of 0.109, which indicated higher in-plane orientation of PI. The birefringence of PI nanocomposite films decreased with the increase of particle content, and the birefringences of PI-S series were smaller than those of PI-L series. Furthermore, the birefringence of PI-S-1 reduced to almost half of that of pristine PI. This indicates that in-plane orientation of PI was disturbed with the incorporation of particles, and the disturbance was more pronounced with small particles.

From NEXAFS spectrum of N K-edge, pristine PI appeared to have a large difference between 20° of incident angle and 90° of incident angle for the σ^* bond orbital resonance of C—N, representing the parallel orientation of imide rings to the in-plane direction. With the increase of particle content, the difference between 90 and 20° decreased, representing the decreasing of orientation of imide rings. The difference between 90 and 20° of the PI-S series was much smaller than those of PI-L series, which was consistent with the results of the birefringences of PI nanocomposites.

References

1. Siegel, R. In Nanonostructure Science and Technology: World Technology Evaluation Center (WTEC) Panel Report on R&D Status and Trends in Nano-Particles, Nanostructured Materials, and Nanodevices; Siegel, R., Hu, E., Roco, M., Eds.; Kluwer: Dordrecht, 1999; Chapter 1, p 1.
2. Ono, K.; Okuda, R.; Ishii, Y.; Kamimura, S.; Oshima, M. J Phys Chem B 2003, 107, 1941.
3. Pileni, M. J Phys Chem 1993, 97, 6961.
4. Pileni, M.; Motte, L.; Petit, C. Chem Mater 1992, 4, 338.
5. Bawendi, M.; Steigerwald, M.; Brus, L. Annu Rev Phys Chem 1990, 41, 477.
6. Petit, C.; Lixon, M.; Pileni, M. J Phys Chem 1993, 97, 12974.
7. Lisiecki, I.; Pileni, M. J Am Chem Soc 1993, 155, 3887.
8. Lisiecki, I.; Pileni, M. J Phys Chem 1995, 99, 5077.
9. Audram, R.; Huguenard, A. U.S. Pat. 4,302,523 (1981).
10. Ziolo, R. U.S. Pat. 4,474,866 (1984).
11. McMichael, R.; Shull, R.; Wartzendruber, L.; Bennett, L.; Watson, R. J Magn Magn Mater 1992, 111, 29.
12. Rosensweig, R. Ferrohydrodynamics; MIT Press: Cambridge, 1985.
13. Pope, N.; Alsop, R.; Chang, Y.; Sonith, A. J Biomed Mater Res 1994, 28, 449.
14. Marchessault, R.; Richard, S.; Rioux, P. Carbohydr Res 1992, 224, 133.
15. Bhatnagar, S. P.; Rosensweig, R. E. J Magn Magn Mater 1995, 149, 198.
16. Kommareddi, N.; Tata, M.; John, V.; McPherson, G.; Herman, M.; Lee, Y.; O'Connor, C.; Akkara, J.; Kaplan, D. Chem Mater 1996, 8, 801.
17. Guerreo, H.; Rosa, G.; Morales, M.; del Monte, F.; Moreno, E.; Levy, D.; Belenguer, T.; Serna, C. Appl Phys Lett 1997, 71, 2698.
18. Niznansky, D.; Rehspringer, J.; Drillon, M. IEEE Trans Magn 1994, 30, 821.
19. Lukehart, C.; Milne, S.; Stock, S.; Shull, R. J Mater Sci Eng A 1995, 204, 176.
20. Nizanasky, D.; Viart, N. J Sol–Gel Sci Technol 1997, 8, 615.
21. Godovsky, D. Adv Polym Sci 2000, 153, 163.
22. Yamazaki, W. In Application of Polyimides to Microelectronics; Makino, D., Ed., American Chemical Society: Washington, DC, 1994; p 81.
23. Kowalczyk, T. J Appl Phys 1994, 76, 2505.
24. Chang, C.; Wei, K.; Chang, Y.; Chen, W. J Polym Res 2003, 10, 1.
25. Chen, Y.; Iroh, Y. Chem Mater 1999, 11, 1218.
26. Ree, M.; Goh, W. H.; Kim, Y. Polym Bull 1995, 35, 215.
27. Moumen, N.; Veillet, P.; Pileni, M. J Magn Magn Mater 1995, 149, 67.
28. Moumen, N.; Pileni, M. J Phys Chem 1996, 100, 1867.
29. Moumen, N.; Pileni, M. Chem Mater 1996, 8, 1128.
30. Feltin, N.; Pileni, M. Langmuir 1997, 13, 3927.
31. Moroi, Y.; Motomura, K.; Matuura, R. J Colloid Interface Sci 1974, 46, 111.
32. Porter, M., Ed. Handbook of Surfactants; Chapman & Hall: Suffolk, 1994.
33. Massart, R. IEEE Trans Magn 1981, 17, 1247.
34. Ree, M.; Shin, T.; Park, Y.; Kim, S.; Woo, S.; Cho, C.; Park, C. J Polym Sci Part B: Polym Phys 1998, 36, 1261.
35. Tien, P.; Ulrich, R.; Martin, R. Appl Phys Lett 1969, 14, 291.
36. Ree, M.; Chu, C.; Goldberg, M. J Appl Phys 1994, 75, 1410.
37. Sprang, N.; Theirich, D. J Surf Coat Technol 1995, 74, 689.
38. Stöhr, J. NEXAFS Spectroscopy; Cullity, B., Ed.; Springer Series in Surface Sciences 25; Springer-Verlag: Berlin, 1992.
39. Petit, C.; Jain, T.; Billoudet, F.; Pileni, M. Langmuir 1994, 10, 4446.
40. Cullity, B. Introduction to Magnetic Materials; Addison-Wesley: Massachusetts, 1972.
41. Rao, B; Rao, K; J Mater Sci 1997, 32, 6049.
42. Rosales, M.; Amano, E.; Cuantle, M.; Valenzuela, R. Mat Sci Eng B 1997, 49, 221.
43. Strunskus, T.; Grunze, M.; Kochendoerfer, G.; Wöll, Ch. Langmuir 1996, 12, 2712.